Journal of Crystal Growth 312 (2010) 1157–1164

Contents lists available at ScienceDirect

Journal of Crystal Growth

journal homepage: www.elsevier.com/locate/jcrysgro

Strain-compensated GaInAs/AlInAs/InP quantum cascade laser materials

Christine A. Wang [a,*], Anish Goyal [a], Robin Huang [a], Joseph Donnelly [a], Daniel Calawa [a], George Turner [a], Antonio Sanchez-Rubio [a], Allen Hsu [b], Qing Hu [b], B. Williams [c]

[a] Lincoln Laboratory, Massachusetts Institute of Technology, 244 Wood Street, Lexington, MA 02420-9108, USA
[b] Research Laboratory of Electronics, Massachusetts Institute of Technology, Cambridge, MA 02139, USA
[c] University of California, Los Angeles, CA 90095, USA

ARTICLE INFO

Available online 11 November 2009

Keywords:
A2. Metalorganic vapor phase epitaxy
A3. Quantum wells
A3. Semiconducting III–V materials
B3. Heterojunction semiconducting devices
B3. Quantum cascade lasers

ABSTRACT

Strain-compensated (SC) GaInAs/AlInAs/InP multiple-quantum-well structures and quantum cascade lasers (QCLs) with strain levels of 1% and as high as 1.5% were grown by organometallic vapor phase epitaxy (OMVPE). The structures were characterized by high-resolution X-ray (HRXRD) diffraction and atomic force microscopy (AFM), and narrow-ridge QCL devices were fabricated. HRXRD and AFM results indicate very high quality materials with narrow satellite peaks, well-defined interference fringes, and a step-flow growth mode for 1% SC materials. A marginal broadening of satellite peaks is measured for 1.5% SC structures, but step-flow growth is maintained. QCLs based on a conventional four-quantum-well double-phonon resonant active region design with nominal 1% SC were grown with doping concentration varied from 1 to 4×10^{17} cm^{-3} in the active region. The performance of ridge lasers under pulsed conditions is comparable to state-of-the-art results for 4.8 μm devices. QCLs with a novel injectorless four-quantum well QCL design and 1.5% SC operated in pulsed mode at room temperature at 5.5 μm.

1. Introduction

Quantum cascade lasers (QCLs) that operate in the mid-infrared (mid-IR) wavelength range are increasingly attractive as light sources for trace gas sensing [1], infrared countermeasures and free-space optical communications. Since their first report in 1994 [2], significant research has led to major improvements in device performance, particularly in room-temperature, continuous-wave, high-power (> 1.6 W), high-efficiency (> 8.8%) QCLs operating at ~4.6 μm [3,4]. QCL emission wavelength is not an intrinsic property of the semiconductor, but a result of sophisticated band structure engineering of layer thickness and alloy composition. The shortest wavelength achievable is determined by the conduction band offset between barrier and quantum-well layers, and in principle, there is no fundamental limit on the long-wavelength side, except for a potential wavelength gap in the optical phonon (Restrahlen) band. In the GaInAs/AlInAs/InP materials system, QCLs are reported to operate over an extremely wide wavelength range and between 3.05 and 80 μm [5,6]. For 3–5 μm emission, the temperature sensitivity and performance of QCLs are greatly improved by the use of strain-compensated (SC) AlInAs/GaInAs/InP materials grown on InP substrates, in which the tensile strain of AlInAs barrier layers is compensated by the compressive strain of the GaInAs quantum-well layers [7]. SC heterostructures provide increased conduction band offset compared to lattice-matched materials so that leakage of electrons in upper energy levels into the continuum and carrier backfilling of lower levels are reduced. For emission at ~4.6–4.8 μm, the typical level of layer strain is ~1% [3,4,8,9], and for 3–4 μm emission, strain levels as high as 1.5% were reported [5,10].

While there are numerous studies detailing QCL structure design and device performance [11–15], there are fewer studies investigating the epitaxial growth of these devices [16–19], and there is particularly limited reporting on the growth of SC materials for QCLs [19]. An understanding of the correlation between growth conditions, material quality, and device characteristics of QCLs is important for both identifying critical aspects of the materials leading to high-performance SC QCLs and for also making further advances.

QCLs are unipolar devices based on tunneling and intersubband transitions in complex semiconductor heterostructures. Laser gain increases via a cascading scheme in which electrons are injected from one stage to the next stage, with 30 to 40 stages comprising a full QCL. One stage in a typical mid-IR SC GaInAs/AlInAs/InP QCL has 20–24 GaInAs quantum-well (QW) and AlInAs barrier layers, some with thicknesses of only a few monolayers. Thus, a QCL can consist of many hundreds to nearly a thousand layers with an active section totaling a thickness of about 2 μm. Ideally,

* Corresponding author. Tel.: +1 781 981 4466; fax: +1 781 981 0122.
E-mail address: wang@ll.mit.edu (C.A. Wang).

0022-0248/$ - see front matter © 2009 Elsevier B.V. All rights reserved.
doi:10.1016/j.jcrysgro.2009.11.005

quantum-well and barrier layer alloy composition and thickness, along with abrupt interfaces are precisely controlled and reproducible from growth of initial layers to the uppermost layers for efficient electron transfer and minimal scattering at interfaces.

This paper discusses some key considerations for the growth and characterization of SC GaInAs/AlInAs/InP QCL materials. The approach is to utililze growth conditions where the epitaxy proceeds in a step-flow growth mode so that abrupt interfaces and precise layer thicknesses might be achieved throughout the whole QCL injector/active region [19]. Organometallic vapor phase epitaxy (OMVPE) was used for the growth of AlInAs/GaInAs/InP SC materials and QCLs with strain levels of 1 and 1.5%. In previous studies on growth of SC multiple-quantum-wells (MQWs) with compressive-GaInAs/tensile-GaInAs and GaInP/InAsP, it was reported that the photoluminescence and interfaces of SC MQWs degraded with increasing layer strain and increasing number of periods [20–22]. Those studies also showed that material quality could be improved by decreasing growth temperature, increasing V/III ratio, and minimizing or eliminating growth interruptions. These growth parameters affect strain-driven adatom surface diffusion such that surface roughening, interface undulations, and composition modulation [23] degrade the MQWs. Even with modifications to growth conditions, good material quality could only be achieved when the strain level was 1% or less. In this study, tertiarybutyl arsine (TBAs) and tertiarybutyl phosphine (TBP) were used as group V precursors in order to enable growth at a lower temperature of 580 °C compared to the more typically used OMVPE temperatures of 650–690 °C when the conventional precursors arsine and phosphine are utilized for QC growth [16,17]. The results presented in this paper show that even these more highly SC (1.5%) AlInAs/GaInAs MQWs and QCLs can be successfully grown by OMVPE under these conditions.

2. Experimental procedure

$Ga_xIn_{1-x}As/Al_yIn_{1-y}As$/InP epilayers were grown by OMVPE in Veeco D125 multi-wafer reactor on nominal (1 0 0) n-InP substrates at a growth temperature of 580 °C with trimethylaluminum (TMAl), trimethylindium (TMIn), triethylgallium (TEGa), tertiarybutyl phosphine, and tertiarybutyl arsine as precursors and Si_2H_6 as the n-type dopant as described previously [19]. GaInAs and AlInAs were grown at growth rates ranging from 0.2 to 0.5 nm/s and a V/III ratio of ~5. A single TMIn source with a constant flow rate was used for both GaInAs and AlInAs, unless specifically stated. The composition of GaInAs and AlInAs was adjusted by changing the TEGa and TMAl flows. As reported earlier, the AlInAs growth rate increased linearly from 0.3 to 0.5 nm/s for lattice-matched to 1.5% tensile strain (y=0.7) layers, respectively, while the GaInAs growth rate was independent of TEGa flow and constant at 0.2 nm/s, i.e. was the same for lattice-matched and 1.5% compressively strained (x=0.25) GaInAs.

To evaluate the suitability of highly SC materials for QCLs, nominally 1.5% SC MQW structures were grown with an extra AlInAs barrier layer as the uppermost layer. Two considerations were studied. One is related to the effect of increasing number of periods, since a QCL laser core is typically 1.5–2 μm thick. The second is the effect of decreasing barrier and QW thickness on interface quality. For the first consideration, a set of 1.5% SC MQWs were grown in which the thickness of the barrier and QW was constant and the number of periods was increased. For the second consideration, a set of 1.5% SC MQWs were grown in which the thickness of the barrier and QW was reduced by half while the number of periods was doubled, thereby keeping the total thickness and cumulative strain energy of the SC MQW constant, but each time doubling the number of interfaces. The thickest SC MQW consisted of 10 and 12.5 nm AlInAs barrier and GaInAs QW layers, respectively, and the number of periods in the MQW was varied from 12 to 36. The AlInAs layer was thinner compared to the GaInAs layer in order to minimize the cumulative net strain. The thinnest SC MQW consisted of 48 periods of 2.5 nm AlInAs and 3.12 nm GaInAs. All heterostructures were grown without growth interruptions. The layers were characterized by atomic force microscopy (AFM) on a Veeco Dimension 5000 AFM operated in tapping mode. High-resolution X-ray diffraction (HRXRD) scans and simulations were performed to determine alloy composition, layer thickness, and to qualitatively evaluate the interface quality.

SC QCL structures with layer strains of 1 and 1.5% were grown. The 1% SC QCL is a conventional design using a four-quantum-well double phonon resonant structure for 4.7 μm emission [8]. One stage of the $Ga_{0.331}In_{0.669}As/Al_{0.638}In_{0.362}As$ layer sequence consists of seven injector well/barrier pairs with the following thicknesses (in nm): (2.8/**1.7**), (2.5/**1.8**), (<u>2.2</u>/**<u>1.9</u>**), (<u>2.1</u>/**<u>2.1</u>**), (2.0/**2.1**), (1.8/**2.7**), and (1.8/**3.8**); and of four active well/barrier pairs: (1.2/**1.3**), (4.3/**1.3**), (3.8,**1.4**), and (3.6/**2.2**). The barrier layers are in bold and the Si-doped layers are underlined. The nominal 1% strain of both barrier and well layers result in strain compensation over one stage. The number of stages is 30. Since QCL performance is sensitive to doping [24,25], the concentration, which is based on bulk GaInAs layers, was varied from 1 to $4\times10^{17}\,cm^{-3}$. The lower and upper InP cladding layer thickness is 3 μm and Si doped at $1\times10^{17}\,cm^{-3}$. Upper and lower GaInAs waveguide layers are Si doped $3\times10^{16}\,cm^{-3}$ and 0.3 μm thick. An upper heavily Si-doped ($>5\times10^{18}\,cm^{-3}$) plasmon-confinement layer is 0.75 μm thick.

A more novel four-well injectorless QCL design [26], which required asymmetrical strain with more highly strained AlInAs barriers to obtain strain compensation, was also grown. The injectorless QCL [27] is designed to provide direct injection of electrons from the ground state to the upper laser level of the subsequent stage without the need of a bridging miniband. This approach has the potential of low voltage defect compared to more conventional designs and injectorless QCLs have been shown to have very low threshold current density [28]. The short period in these injectorless structures requires a large electric field necessitating as large a band offset as possible. The four-well structure utilized $Ga_{0.35}In_{0.65}As/Al_{0.70}In_{0.30}As$, corresponding to 0.81% compressive strain in the wells and 1.54% tensile strain in the barriers, to provide an estimated conduction band offset close to 0.9 eV. The asymmetric strain is required to obtain overall strain-compensation since the total thicknesses of the GaInAs layers in each period is substantially larger than that of the AlInAs layers. From a growth perspective, the high strain in the AlInAs barriers make this structure extremely challenging. The layer sequence of one stage starting with the injection barrier was **<u>32</u>**/24/**19**/55/**13**/41/**<u>15</u>**/<u>32</u>, where the bold layers are $Al_{0.70}In_{0.30}As$ and the underlined layers are n-doped $4\times10^{17}\,cm^{-3}$. The number of stages is 45. The cladding, waveguide, and plasmon layers were the same as that used for the 1% SC QCL. To simplify materials characterization of SC QCL structures, cladding, confining, and plasmon layers were omitted and only the QCL laser core was grown with a thin InP cap layer.

Ridge-waveguide lasers were fabricated from the QCL material using conventional photolithography and $SiCl_4$-based inductively coupled plasma dry-etching. After forming the laser ridges by etching through the active region, a 0.3-μm-thick film of SiO_2 was blanket-deposited for electrical insulation. To contact the top of the laser ridges, openings were made in the SiO_2 using CF_4 reactive ion etching and Ti–Au metallization was evaporated and patterned. After the wafer was thinned, metal contacts were deposited on the backside to form the substrate contact. Unless otherwise stated, devices were then cleaved into bars. In some

cases, high reflectivity (HR) facet coatings (SiO_2/Ti/Au/Ti/SiO_2) were applied to the back facets. The lasers were mounted ridge-side up in bar form onto a copper submount using indium solder.

Laser testing was performed under both pulsed and continuous-wave (CW) conditions. For pulsed measurements the pulse duration was typically 100–200 ns at a repetition frequency of 1 kHz. For measurements made near room temperature, devices were attached to a thermoelectrically cooled stage. The laser power was directly coupled into an integrating sphere with HgCdTe detector (Vigo PCI-3TE-12). Power calibration of the photodetector signal was made by measuring the laser power using a thermal detector. For low-temperature measurements, lasers were mounted in a liquid nitrogen (LN_2) crystostat and the laser power was coupled to the integrating sphere using an $f/1$ CaF_2 lens. For CW measurements, the laser power was measured using a thermal detector in combination with a Winston cone. In all cases, the collected power is reported and no correction is made for collection efficiency. The lasing wavelength was measured using a grating spectrometer.

3. 1 and 1.5% GaInAs/AlInAs SC MQWs and SC QCL materials results

A combination of HRXRD analyses and AFM was used to determine alloy composition, layer thickness, and to qualitatively evaluate the interface quality. As a baseline starting point, a growth rate of ~0.2 nm/s and V/III=5 were established as described [19] to obtain a step-flow growth mode for lattice-matched (LM) GaInAs, LM AlInAs, and LM MQWs (50 nm AlInAs barrier layers and GaInAs quantum wells with thickness varying from 10 to 80 nm). AFM images (5×5 μm scan) in Fig. 1 show surface steps that run diagonally across the image, which is indicative that the growth proceeds in a step-flow mode. LM GaInAs has a surface root-mean-square (RMS) roughness of ~0.15 nm. The RMS roughness of LM AlInAs is slightly higher at ~0.27 nm, and the RMS roughness of a typical LM MQW is ~0.23 nm. As a reference point, RMS roughness of InP is 0.09 nm. These results show that the individual layers have monolayer step heights that can be propagated in MQW structures, and that the roughness in LM MQWs is dominated by that of the AlInAs.

Next, 1.5% SC MQWs were grown and the growth mode was compared to LM materials. Fig. 2 shows the AFM image (1×1 μm scan) of a 36-period 1.5% SC MQW with 10 nm AlInAs barrier and 12.5 nm GaInAs QW layers. The total thickness of the structure is 0.8 μm. As can be seen, step flow is achieved even with this very high level of layer strain. The RMS roughness is only 0.121 nm, and is 0.118 nm for a 12-period structure. For a 10×10 μm scan, the RMS roughness only increased to 0.16 nm. These values are slightly less than that measured for LM MQWs and may be explained by the reduced AlInAs barrier layer thickness in the SC MQWs. Thus, under the presently described growth conditions, there is no degradation in the atomic step structure of 1.5% SC MQWs, and the surface remains stable from the onset of growth until the end, with no indication of strain-induced surface modulation [22]. It is noted that the orientation of the steps shown in Fig. 2 are aligned more parallel to the [1 1 0]. This is a consequence of the small InP substrate miscut, which was slightly different than the substrates used for the samples shown in Fig. 1.

HRXRD scans and simulations are very important characterization tools to quantitatively determine layer strain and thickness, as well as provide insight into the overall quality of

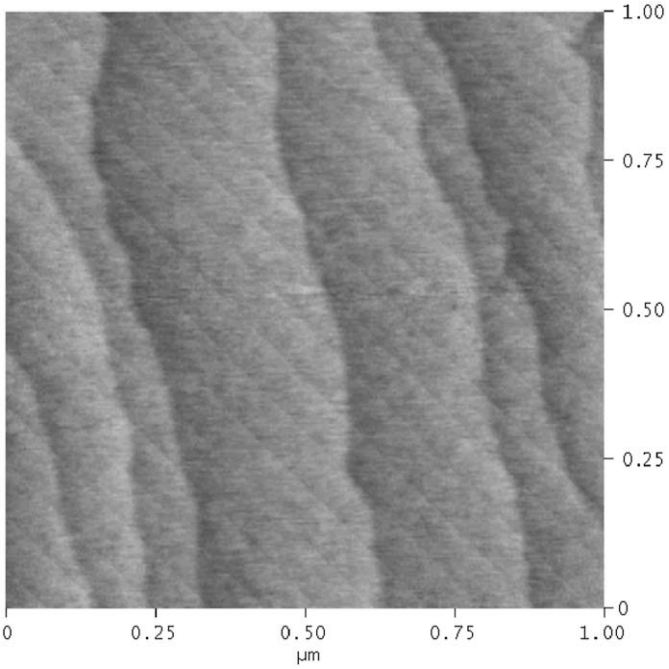

Fig. 2. Atomic force microscopy image (1×1 μm) of 36-period 10 nm barrier/12.5 nm well 1.5% SC MQW.

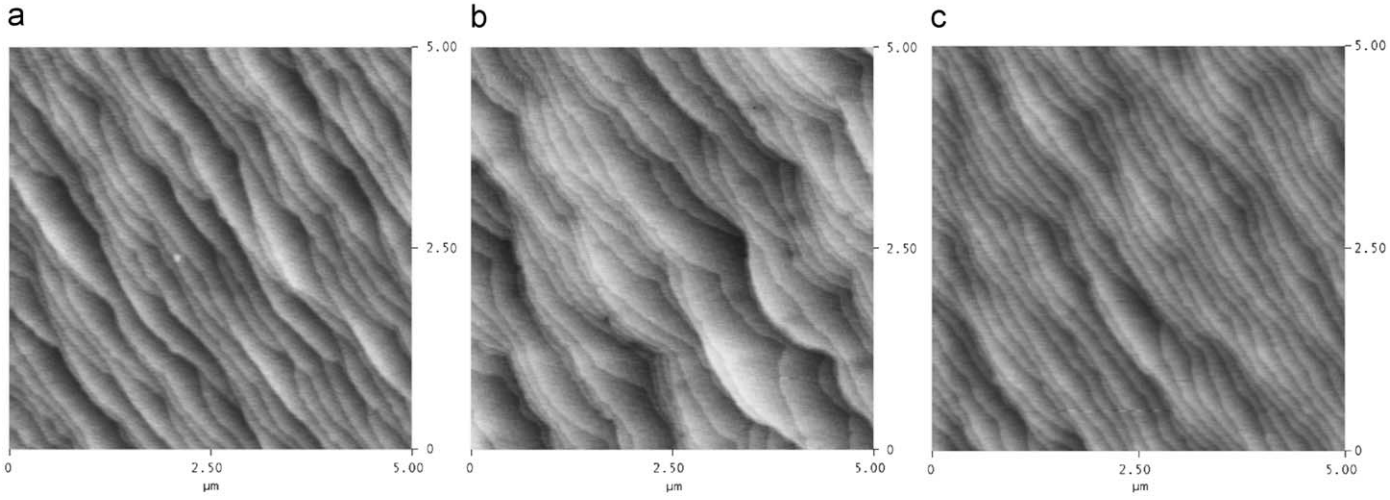

Fig. 1. Atomic force microscopy images (5×5 μm scan) of 0.3-μm-thick (a) LM GaInAs, (b) LM AlInAs and (c) LM GaInAs/AlInAs MQW.

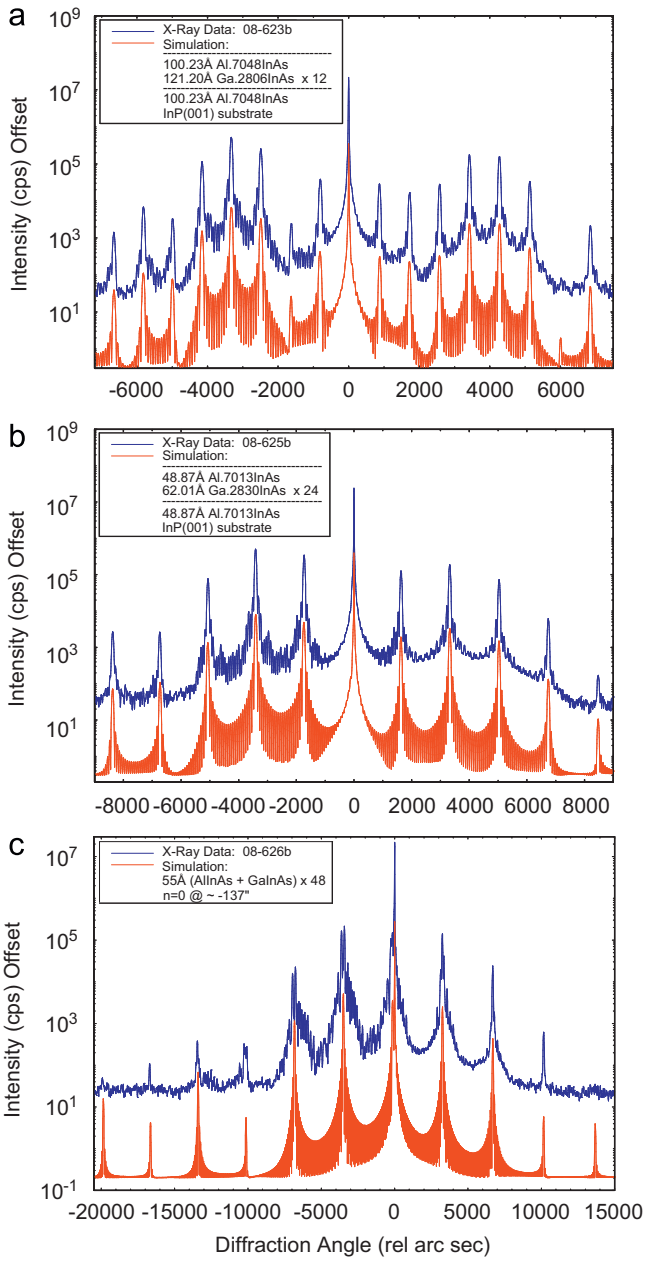

Fig. 3. High-resolution X-ray diffraction scans and simulations of 1.5% SC MQWs: (a) 12-period 10 nm barrier/12.5 nm well, (b) 24-period 5 nm barrier/6.25 nm well and (c) 48-period 2.5 nm barrier/3.12 nm well.

interfaces. Fig. 3 shows HRXRD scans and simulations of a series of 1.5% SC MQWs in which the barrier/well layer thickness was systematically reduced by half while the number of periods was doubled. The baseline structure consisted of 10 nm barrier layers, 12.5 nm QWs, and 12 periods. The 48-period SC MQW consists of 2.5 nm barriers and 3.12 nm wells, which are similar to layer thicknesses used in QCLs. The simulation of the 12-period structure (Fig. 3a) shows satellite peaks and envelopes on the compressive and tensile side of the scan. The satellites determine the periodicity of the MQW while the position and width of the envelopes determine the alloy composition and individual layer thickness, respectively. It should be noted that a unique simulation of composition and thickness for the 48 period MQW (Fig. 3c) cannot be determined because the very thin layers result in broad envelope widths that overlap. The position of the $n=0$ peak, which is a measure of the average lattice constant was +44, −49, and −137 arc s for the 12-, 24-, and 48-period MQWs, respectively. The satellite peaks are narrow and interference fringes are well-defined for the 12- and 24-period SC MQWs, and are in line with XRD simulations. However, broadening of satellite peaks especially on the compressive side is observed for the 48-period SC MQW with the thinnest layers. We confirmed that such broadening was not observed for a 1% SC MQW with the same number of periods and barrier/well thickness, even with an $n=0$ peak at −470 arc s, which corresponds to a residual structure strain of 0.2%. The HRXRD for this sample is shown in Fig. 4. While the reason for broadening on the compressive side for the thinnest layers is unclear at this time, these results show that it is possible to grow very high quality and nearly ideal SC structures even with layer strain as high as 1.5% as long as the barrier/well layers are ~5–6 nm or thicker, and only slight deterioration is observed for ~2–3 nm layers.

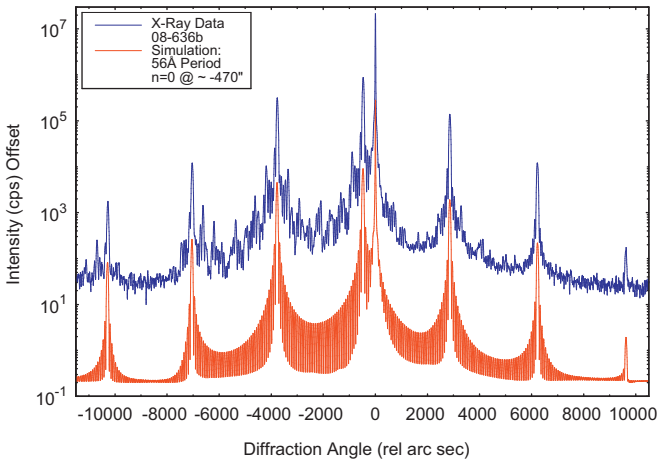

Fig. 4. High-resolution X-ray diffraction scans and simulation of a 48-period 2.5 nm barrier/3.12 nm well 1% SC MQW.

As mentioned in Section 2, the growth rate of AlInAs increased with increasing Al content (tensile strain), since the TMIn flow was constant and TMAl flow was increased. The use of a high rate of 0.5 nm/s for AlInAs for growth of QCL structures, in which AlInAs layer thickness is <2 nm, will result in more interface grading than if a lower growth rate is used. This is due to convective dispersion in rotating-disk OMVPE reactors [29]. To investigate the effect of lower growth rate on interface quality, in another set of experiments, both TMIn and TMAl flow rates were lowered. Since only one TMIn source was used, both AlInAs and GaInAs rates were reduced by about half. 1.5% SC MQWs were grown with reduced AlInAs and GaInAs growth rates of 0.25 and 0.1 nm/s, respectively. The HRXRD scan shows major broadening of satellite peaks and no interference fringes, while AFM imaging revealed an irregular surface structure and RMS surface roughness of 19 nm. It was subsequently determined in AFM studies that the step edges of GaInAs and AlInAs grown at these low rates is very irregular. These results confirm the importance of maintaining step-flow growth and monoatomic step heights for growth of high quality SC MQWs.

Test 1% and 1.5% SC QCL structures were grown with injector/active regions as described in Section 2. In these test structures, the upper waveguide and cladding layers were omitted, and the structures were capped with a thin (~8 nm) InP layer to observe the growth mode. AFM images confirmed step-flow growth is observed with RMS roughness <0.2 nm for 10×10 μm scans.

HRXRD of the 1% and 1.5% SC QCLs are shown in Figs. 5a and c, respectively. There was no significant change in the HRXRD for the 1% SC QCLs with various doping levels, as one would expect

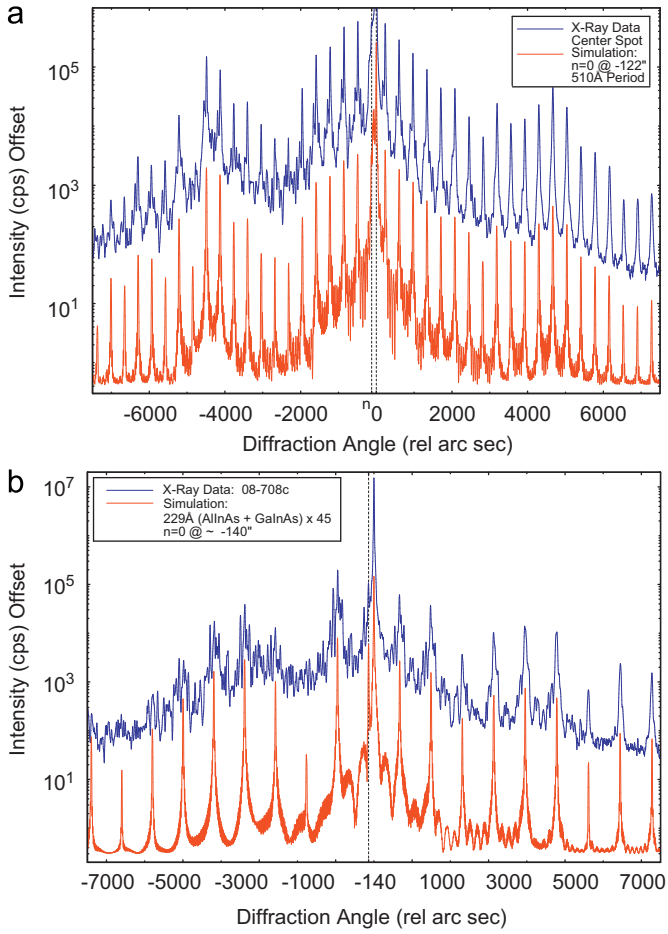

Fig. 5. High-resolution X-ray diffraction scans and simulations of (a) 1% SC QCL and (b) 1.5% SC QCL.

since the doping level is only in the $10^{17}\,cm^{-3}$ range. The XRD spectra are complex due to the QCL regions with many thin layers and the strain compensation. The intended QCL period is 50.4 and 23.1 nm for the ~1 and ~1.5% structures, respectively, and the extracted period from the HRXRD is 50.9 and 22.9 nm. The observance of sharp satellites with good intensity is indicative of excellent depth uniformity, control of layer thickness and composition, and interfaces throughout the structure. As was observed for the 1.5% SC MQW with the thinnest layers (Fig. 3c), the satellites on the compressive side are somewhat broadened. In general, though, the good agreement between the two spectra confirms the ability to grow highly SC QCLs.

4. 1 And 1.5% SC QCL Devices

The effect of injector doping level on SC QCL performance was investigated for the 1% SC QCLs with four different doping levels of nominally 1×10^{17}, 2×10^{17}, 3×10^{17}, and $4\times10^{17}\,cm^{-3}$. The room temperature lasing wavelength was 4.8 μm for all four laser wafers. In one series of experiments, 4-mm-long devices from each wafer were characterized as a function of temperature from 78 K to 300 K. Fig. 6 shows a typical *L–I–V* (light–current–voltage) measurement as a function of temperature. A variety of parameters were extracted. These included the threshold current density, J_{th}; the slope efficiency (power from both facets); the operating current at maximum laser power, J_{max}; the operating voltage at maximum laser power, V_{max}; and the

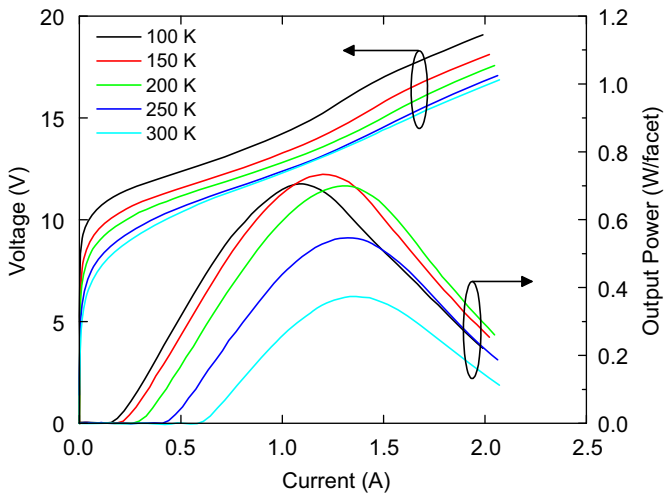

Fig. 6. Pulsed *L–I–V* characteristics of 1% SC QCL (4 mm × 8 μm device) with a layer doping of $4\times10^{17}\,cm^{-3}$ (07–627) as a function of temperature.

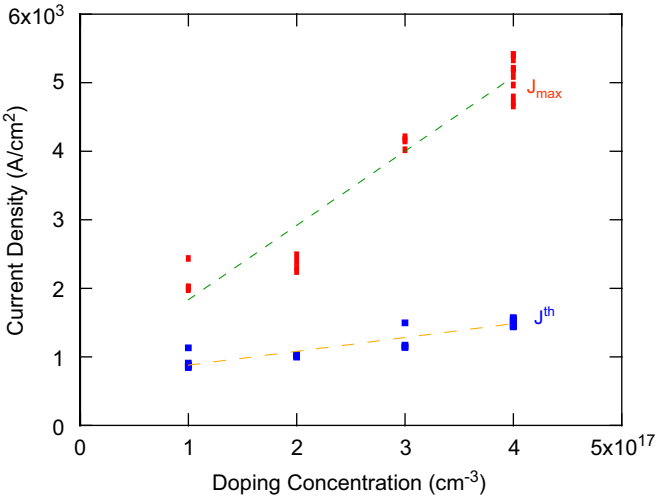

Fig. 7. J_{th} and J_{max} at 288 K for 1% SC QCL (4-mm-long devices) as a function of injector doping concentration. Measurements were made on unmounted bars under pulsed conditions.

differential resistance, ρ. As shown in Fig. 7, the lowest doped device ($n=1\times10^{17}\,cm^{-3}$) had a threshold current density of only 842 A/cm^2 at 288 K. The increase in J_{th} with doping is presumably due to an increase in waveguide losses. The waveguide loss was determined by measuring the threshold of a particular device both before and after HR facet coating and assuming that the modal gain is directly proportional to the current density. For a device having an injector doping of $1\times10^{17}\,cm^{-3}$, one calculates a very low waveguide loss of $1.34\,cm^{-1}$. The waveguide loss was found to increase monotonically with doping. Fig. 7 also shows the strong dependence of J_{max} on doping level. This can be understood from the observations that the differential resistance, ρ, decreased with increasing injector doping whereas V_{max} remains relatively constant. The ρ was found to be independent of temperature except for the lowest doped samples for which ρ increased significantly below 150 K; this behavior is attributed to freeze-out of the carriers in the injector. Fig. 8 shows the dependence of J_{th} and the slope efficiency (power from both facets) as a function of temperature. The characteristic temperature was found to be independent of injector doping

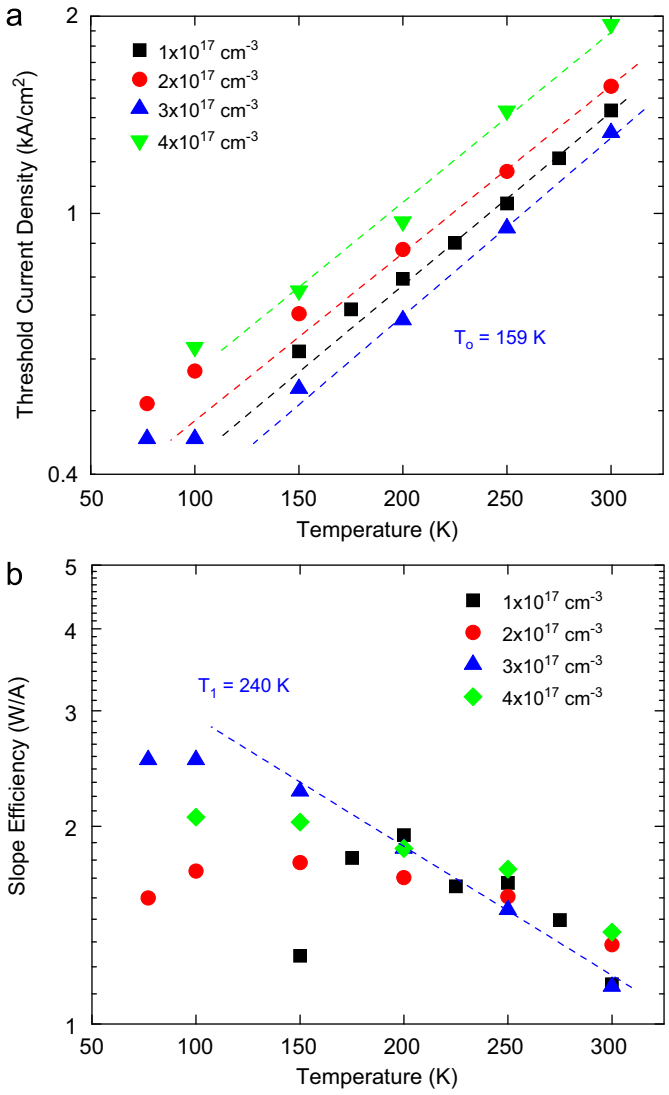

Fig. 8. Threshold current density (a) and pulsed slope-efficiency (b) versus temperature for 1% SC QCL devices of various injector doping concentrations. Except as noted, the devices are 4 mm × 8 μm with uncoated facets.

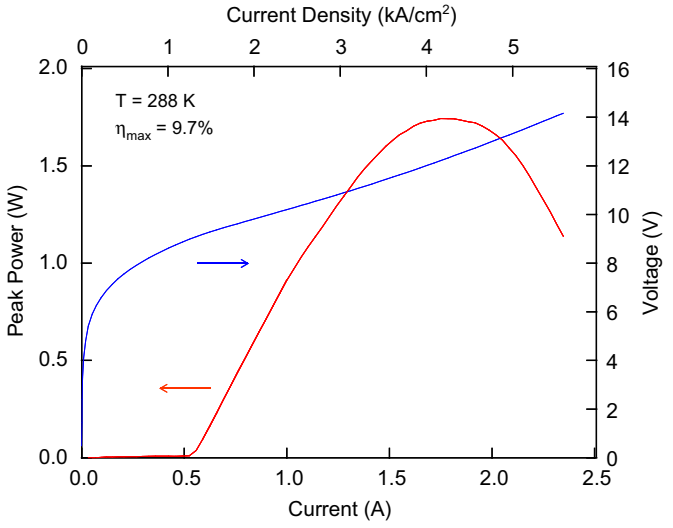

Fig. 9. Pulsed *L–I–V* characteristics for a 1% SC QCL (3 mm × 14 μm device) at T=288 K with an HR-coated facet. The peak power is 1.7 W and the maximum wall-plug efficiency is 9.7%.

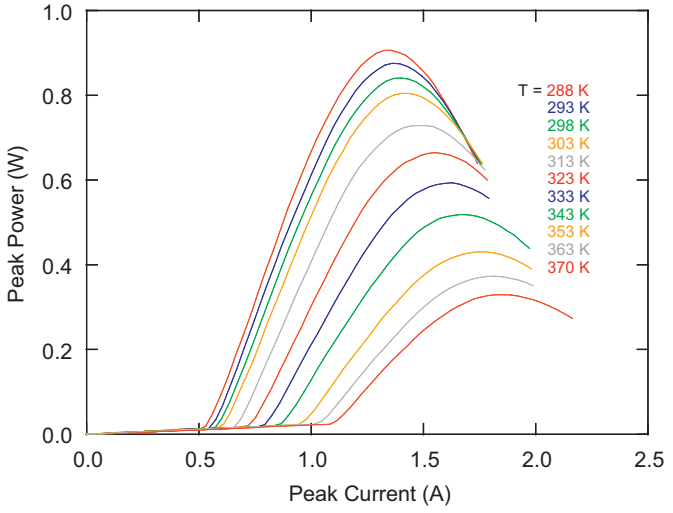

Fig. 10. Pulsed *L–I* characteristics for a 1% SC QCL (3 mm × 14 μm device) with an HR-coated facet. Lasing is observed up to 97 °C. Lasing is extrapolated to occur up to a heat sink temperature of ~150 °C.

level and equal to T_o=159 K. The slope efficiency decreases only moderately as the temperature increases from 100 K to 300 K with T_1=240 K. Given the experimental uncertainties, we do not find a significant difference in the slope efficiency near room temperature for the various injector doping levels. At low temperatures, the most lightly doped samples exhibit a low slope efficiency because of carrier freeze-out as mentioned above.

The *L–I–V* characteristics of a 1% SC QCL with an injector doping of 3×10^{17} cm^{-3} measured at 288 K are shown in Fig. 9. The device had a ridge width of 14 μm and a cavity length of 3 mm. The threshold current density J_{th} of approximately 1.3 kA/cm^2, maximum power conversion efficiency η_{max} of 9.7% (slope efficiency of 2.0 W/A), and peak power of approximately 1.74 W compare favorably to those measured previously for QCLs of the same design. Fig. 10 shows a 1% SC QCL operating at a heat sink temperature of up to 97 °C under pulsed conditions. Lasing is extrapolated to occur up to a heat sink temperature of ~150 °C. These results are consistent with previously reported QCLs of the same design [8] that were grown by MBE, although in that reference, the reported results were obtained for buried heterostructure lasers with reduced thermal resistance and dissipated power, allowing for CW operation close to room temperature. The pulsed results of the ~1% SC QCL reported here and grown by OMVPE suggest the potential for similar power and efficiency performance. Initial efforts were made to improve the thermal dissipation in the devices by electroplating a thick layer of Au over the laser ridge. An 8 μm × 4 mm device with HR facet-coating and electroplated metallization produced 108 mW CW at T=278 K. The maximum heat sink temperature for CW operation was >303 K. Additional work on buried heterostructure lasers [30,8], or electroplated metal ridge waveguide lasers [31,32], of these OMVPE-grown QCLs is required in order to improve the thermal performance at high average powers close to room temperature and make a more direct comparison.

Fig. 11 shows the *L–I–V* characteristics of a the injectorless 1.5% SC QCL. The 8-μm wide ridge device is 3-mm long with uncoated facets. These devices lased when operated in pulsed mode at temperatures up to 300 K. Laser emission was at

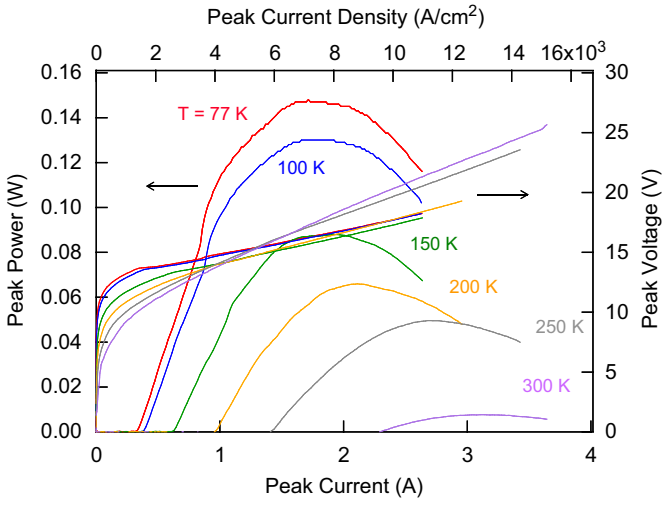

Fig. 11. Pulsed *L–I–V* characteristics of 1.5% SC injectorless QCL at temperatures from 77 to 300 K.

~5.6 μm. At 77 K, J_{th} is 1.4 kA/cm^2 and the voltage defect is 77 mV at threshold and 103 mV at the point of maximum power conversion efficiency. The slope efficiency is 0.492 W/A and a peak power is 444 mW. Further work on optimizing the design, growth and fabrication procedures for this novel QCL structure should lead to improved device performance in threshold current, operating temperature and power output.

5. Summary

SC GaInAs/AlInAs/InP MQWs and QCL with strain levels of 1% and as high as 1.5% were grown with by OMVPE. A step-flow growth mode is important for obtaining high quality structures as characterized by HRXRD with narrow satellite peaks and good definition of interference fringes. Monoatomic step heights aid in achievement of precise thickness control, which is required for SC QCL injector/active designs. The 1% SC QCLs are consistent with state-of-the-art QCL performance with very low J_{th} of 842 A/cm^2 at 288 K and very low waveguide loss of 1.34 cm^{-1}. Higher levels of strain were investigated for a novel injectorless QCL, whose performance depends critically on high conduction band offsets. SC injectorless QCLs with 1.5% AlInAs barrier layers and 0.8% GaInAs QWs operated .in pulsed mode at room temperature.

Acknowledgments

The authors express their appreciation to, D. McNulty for assistance in growth, S.G. Cann for AFM characterization, and M.K. Connors, L.J. Missaggia, F. O'Donnell, and J.J. Plant for fabrication. This work was sponsored by DARPA and the Department of the Air Force under Air Force contract number FA8721-05-C-0002. The opinions, interpretations, conclusions and recommendations are those of the authors and are not necessarily endorsed by the United States government.

References

[1] A. Kosterev, G. Wysocki, Y. Bakhirkin, S. So, R. Lewicki, M. Fraser, F. Tittel, R.F. Curl, Application of quantum cascade lasers to trace gas analysis, Applied Physics B: Lasers and Optics 90 (2008) 165–176.
[2] J. Faist, F. Capasso, D.L. Sivco, C. Sirtori, A.L. Hutchinson, A.Y. Cho, Quantum Cascade Laser, Science 264 (1994) 553–556.
[3] A. Lyakh, C. Pflugl, L. Diehl, Q.J. Wang, F. Capasso, X.J. Wang, J.Y. Fan, T. Tanbun-Ek, R. Maulini, A. Tsekoun, R. Go, C.K.N. Patel, 1.6 W high wall plug efficiency, continuous-wave room temperature quantum cascade laser emitting at 4.6 mu m, Applied Physics Letters 92 (2008) 111110-3.
[4] Y. Bai, S. Slivken, S.R. Darvish, M. Razeghi, Room temperature continuous wave operation of quantum cascade lasers with 12.5% wall plug efficiency, Applied Physics Letters 93 (2008) 021103-3.
[5] M.P. Semtsiv, M. Wienold, S. Dressler, W.T. Masselink, Short-wavelength (λ~3.05 μm) InP-based strain-compensated quantum-cascade laser, Applied Physics Letters 90 (2007) 051111-3.
[6] M. Fischer, G. Scalari, C. Walther, J. Faist, Terahertz quantum cascade lasers based on In0.53Ga0.47As/In0.52Al0.48As/InP, Journal of Crystal Growth 311 (2009) 1939–1943.
[7] J. Faist, F. Capasso, D.L. Sivco, A.L. Hutchinson, S.-N.G. Chu, A.Y. Cho, Short wavelength (λ~3.4 μm) quantum cascade laser based on strained compensated InGaAs/AlInAs, Applied Physics Letters 72 (1998) 680–682.
[8] A. Evans, S.R. Darvish, S. Slivken, J. Nguyen, Y. Bai, M. Razeghi, Buried heterostructure quantum cascade lasers with high continuous-wave wall plug efficiency, Applied Physics Letters 91 (2007) 071101-3.
[9] X.J. Wang, J.Y. Fan, T. Tanbun-Ek, F.-S. Choa, Low threshold quantum-cascade lasers of room temperature continuous-wave operation grown by metal-organic chemical-vapor deposition, Applied Physics Letters 90 (2007) 211103-3.
[10] J.S. Yu, S.R. Darvish, A. Evans, J. Nguyen, S. Slivken, M. Razeghi, Room-temperature continuous-wave operation of quantum-cascade lasers at lambda ~4 μm, Applied Physics Letters 88 (2006) 041111-3.
[11] F. Capasso, A. Tredicucci, C. Gmachl, D.L. Sivco, A.L. Hutchinson, A.Y. Cho, G. Scamarcio, High-performance superlattice quantum cascade lasers, IEEE Journal of Selected Topics in Quantum Electronics 5 (1999) 792–807.
[12] C. Gmachi, F. Capasso, A. Tredicucci, D.L. Sivxo, R. Kohler, A.L. Hutchinson, A.Y. Cho, Dependence of the device performance on the number of stages in quantum-cascade lasers, IEEE Journal of Selected Topics in Quantum Electronics 5 (1999) 808–816.
[13] K. Faist, D. Hofstetter, M. Beck, T. Aellen, M. Rochat, S. Blaser, Bound-to-continuum and two-phonon resonance, quantum-cascade lasers for high duty cycle, high-temperature operation, IEEE Journal of Quantum Electronics 38 (2002) 533–546.
[14] J.S. Yu, S. Slivken, A.J. Evans, M. Razeghi, High-performance continuous-wave operation of λ~4.6 μm quantum-cascade lasers above room temperature, IEEE Journal of Quantum Electronics 44 (2008) 747–754.
[15] W. T. Masselink, M. P. Semtsiv, M. Wienold, M. Chashnikova, I. Bayrakli, and M. Klinkmuller, Strain-compensated AlAs-InGaAs quantum-cascade lasers with emission wavelength 3–5 mu m, presented at Physics and Simulation of Optoelectronic Devices XVI, San Jose, CA, USA, 2008.
[16] A.B. Krysa, J.S. Roberts, R.P. Green, L.R. Wilson, H. Page, M. Garcia, J.W. Cockburn, MOVPE-grown quantum cascade lasers operating at ~9 μm wavelength, Journal of Crystal Growth 272 (2004) 682–685.
[17] D. Bour, M. Troccoli, F. Capasso, S. Corzine, A. Tandon, D. Mars, G. Hofler, Metalorganic vapor-phase epitaxy of room-temperature, low-threshold InGaAs/AlInAs quantum cascade lasers, Journal of Crystal Growth 272 (2004) 526–530.
[18] A.Z. Li, H. Li, G.Y. Xu, Y.G. Zhang, C. Lin, C. Zhu, L. Wei, Y.Y. Li, Key issues associated with low threshold current density for InP-based quantum cascade lasers, Journal of Crystal Growth 301–302 (2007) 129–133.
[19] C.A. Wang, R.K. Huang, A. Goyal, J.P. Donnelly, D.R. Calawa, S.G. Cann, F. O'Donnell, J.J. Plant, L.J. Missaggia, G.W. Turner, A. Sanchez-Rubio, OMVPE growth of highly strain-balanced GaInAs/AlInAs/InP for quantum cascade lasers, Journal of Crystal Growth 310 (2008) 5191–5197.
[20] T. Tsuchiya, M. Komori, R. Tsuneta, H. Kakibayashi, Investigation of effect of strain-compensated structure and compensation limit in strained-layer multiple quantum wells, Journal of Crystal Growth 145 (1994) 371–375.
[21] A.D. Smith, A.T.R. Briggs, K. Scarrott, X. Zhou, U. Bangert, Optimization of growth conditions for strain compensated Ga[sub 0.32]In[sub 0.68]As/Ga[sub 0.61]In[sub 0.39]As multiple quantum wells, Applied Physics Letters 65 (1994) 2311–2313.
[22] P. Desjardins, H. Marchand, L. Isnard, R.A. Masut, Microstructure and strain relaxation in organometallic vapor phase epitaxy of strain-compensated GaInP/InAsP multilayers on InP(0 0 1), Journal of Applied Physics 81 (1997) 3501–3511.
[23] D.M. Follstaedt, R.D. Twesten, J. Mirecki Millunchick, S.R. Lee, E.D. Jones, S.P. Ahrenkiel, Y. Zhang, A. Mascarenhas, Spontaneous lateral composition modulation in InAlAs and InGaAs short-period superlattices, Physica E: Low-dimensional Systems and Nanostructures 2 (1998) 325–329.
[24] T. Aellen, M. Beck, N. Hoyler, M. Giovannini, J. Faist, E. Gini, Doping in quantum cascade lasers. I. InAlAs–InGaAs/InP midinfrared devices, Journal of Applied Physics 100 (2006) 043101-4.
[25] E. Mujagic, M. Austerer, S. Schartner, M. Nobile, L.K. Hoffmann, W. Schrenk, G. Strasser, M.P. Semtsiv, I. Bayrakli, M. Wienold, W.T Masselink, Impact of doping on the performance of short-wavelength InP-based quantum-cascade lasers, Journal of Applied Physics 103 (2008) 033104–4.
[26] A. Hsu, Q. Hu, and B. Williams, Four-Well Highly Strained Quantum Cascade Lasers Grown by Metal-Organic Chemical Vapor Deposition, presented at CLEO, 2009.
[27] A. Friedrich, C. Huber, G. Boehm, M.-C. Amann, Low-threshold room-temperature operation of injectorless quantum-cascade lasers: influence of doping density, Electronics Letters 42 (2006) 1228–1229.

[28] G. Boehm, S. Katz, R. Meyer, M.-C. Amann, Al(In)As-(Ga)InAs strain-compensated active regions for injectorless quantum cascade lasers, Journal of Crystal Growth 311 (2009) 1932–1934.
[29] C.A. Wang, S. Patnaik, J.W. Caunt, R.A. Brown, Growth characteristics of a vertical rotating-disk OMVPE reactor, Journal of Crystal Growth 93 (1988) 228–234.
[30] M. Beck, J. Faist, U. Oesterle, M. Ilegems, E. Gini, H. Melchior, Buried heterostructure quantum cascade lasers with a large optical cavity waveguide, IEEE of Photonics Technology Letters 12 (2000) 1450–1452.
[31] A. Evans, J.S. Yu, S. Slivken, M. Razeghi, Continuous-wave operation of lambda$\sim$4.8 mu m quantum-cascade lasers at room temperature, Applied Physics Letters 85 (2004) 2166–2168.
[32] Z. Liu, D. Wasserman, S.S. Howard, A.J. Hoffman, C.F. Gmachl, X. Wang, T. Tanbun-Ek, L. Cheng, F.-S. Choa, Room-temperature continuous-wave quantum cascade lasers grown by MOCVD without lateral regrowth, IEEE Photonics Technology Letters 18 (2006) 1347–1349.